

Fig. S2 XPS spectra of Ti, O and K in sample $K_2Ti_4O_9$ -CdS-1.

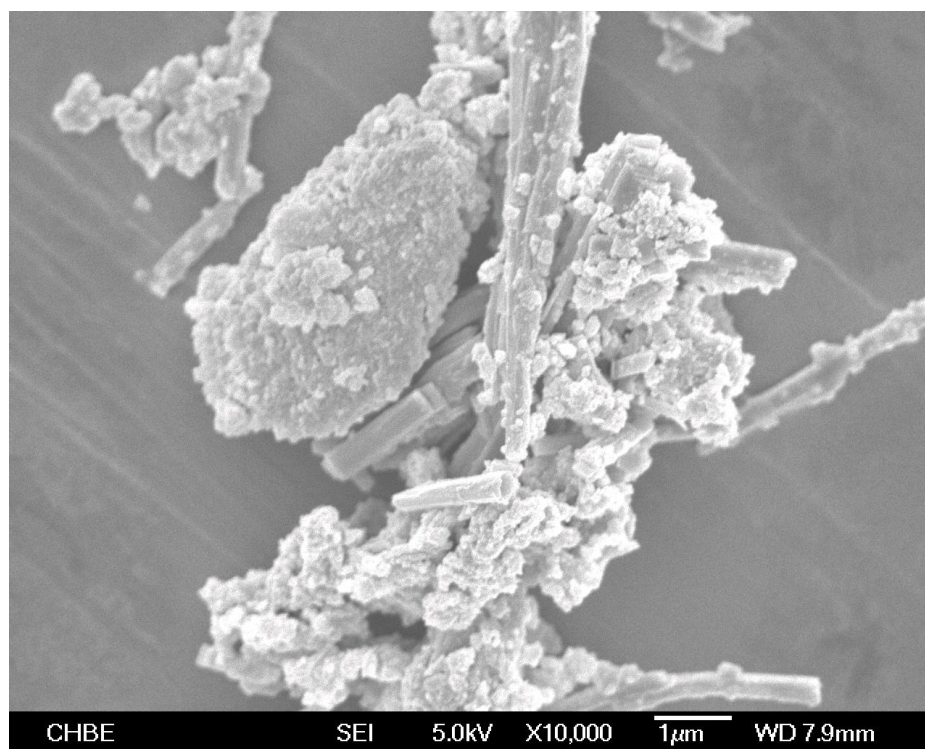


Fig. S3 FESEM image of sample $(K_2Ti_4O_9-CdS)_{mix}$.

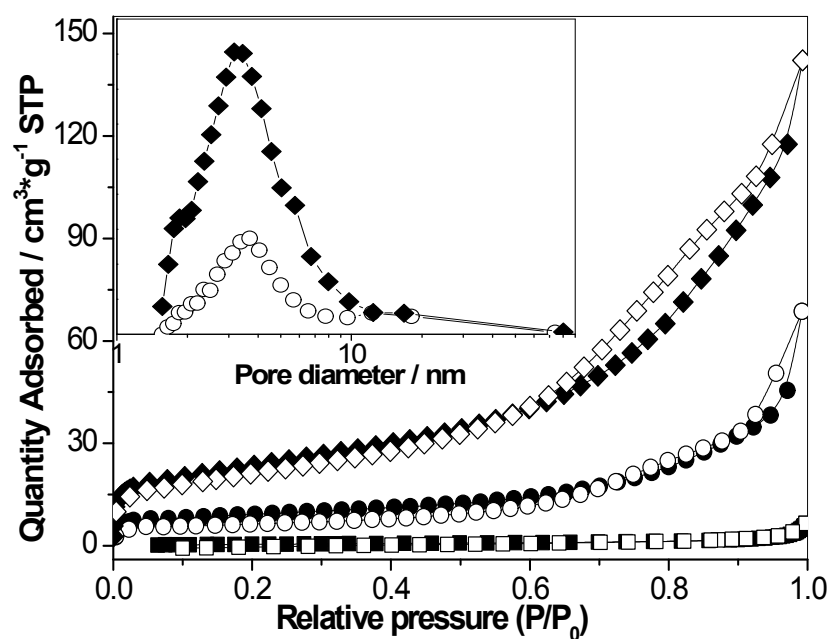


Fig. S4 N_2 adsorption (solid)-desorption (hollow) isotherms of $K_2Ti_4O_9$ (square), $K_2Ti_4O_9-CdS19\%$ (circle) and $K_2Ti_4O_9-CdS47\%$ (diamond), and the pore size distributions (inset) of $K_2Ti_4O_9-CdS19\%$ (circle) and $K_2Ti_4O_9-CdS47\%$ (diamond).

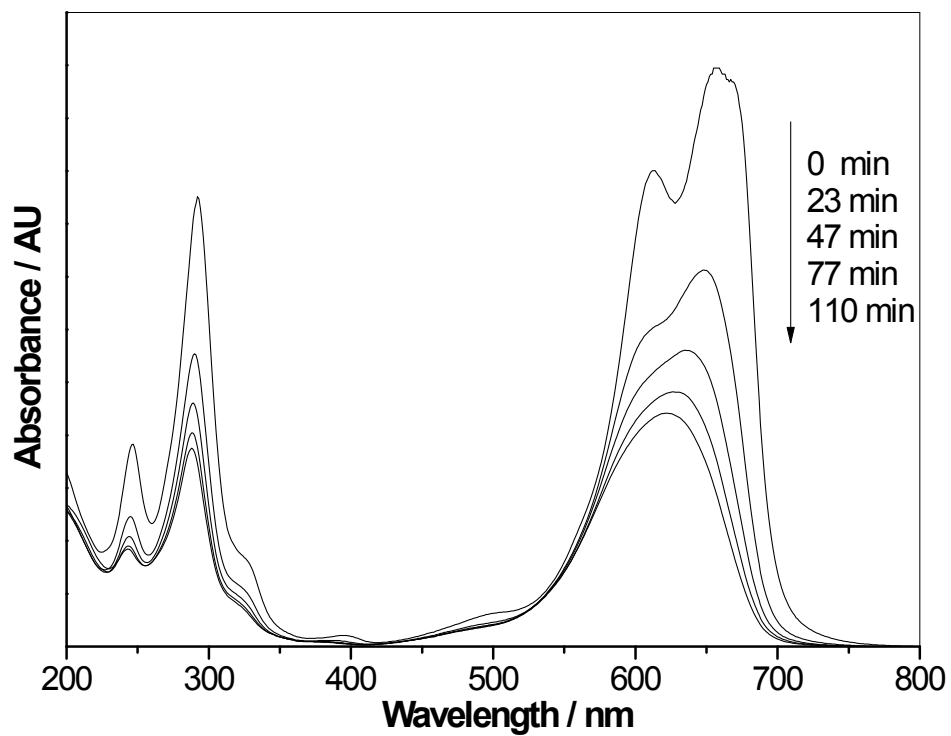


Fig. S5 Absorption spectra of MB with irradiation time over $K_2Ti_4O_9$ -CdS47%.

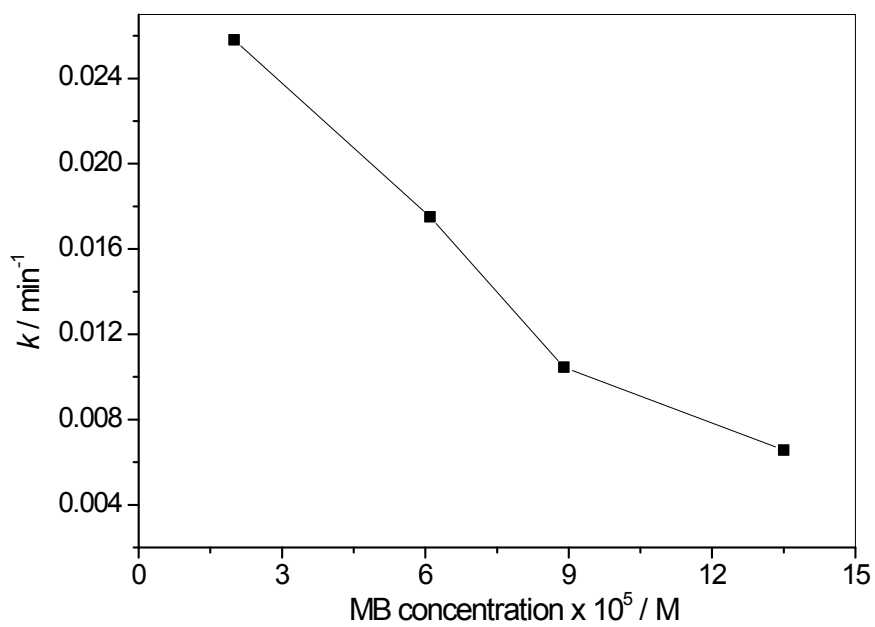


Fig. S6 Effect of initial MB concentration on the rate constant over $K_2Ti_4O_9$ -CdS47%.

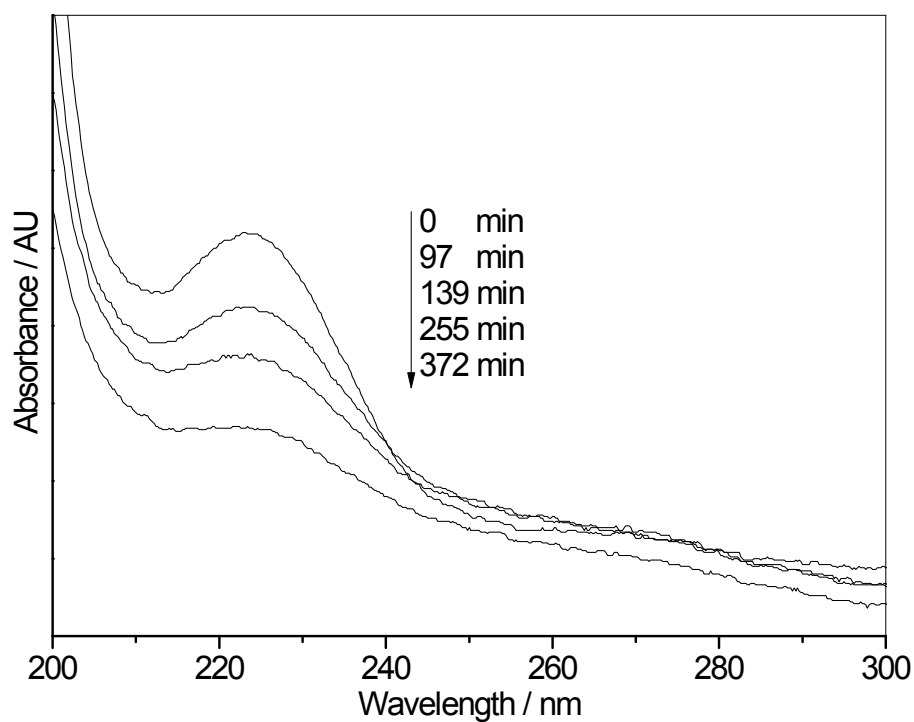


Fig. S7 Absorption spectra of benzoic acid with irradiation time over $K_2Ti_4O_9-CdS47\%$.

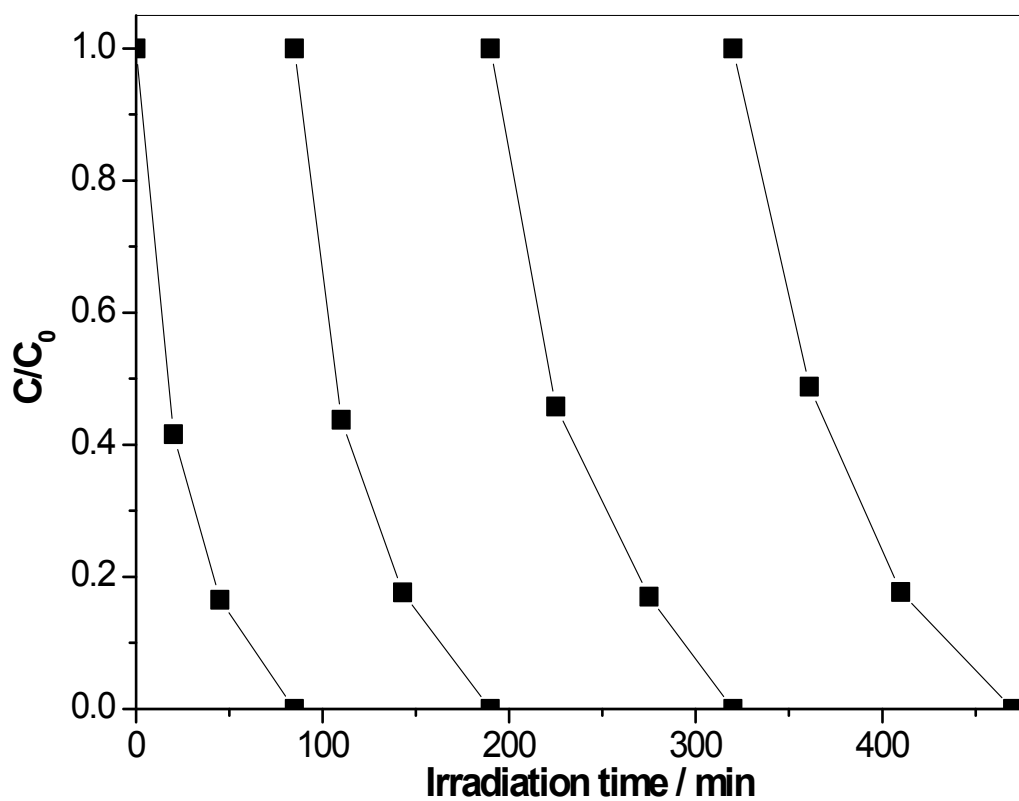


Fig. S8 Repeated photocatalytic degradation of MB over composite $K_2Ti_4O_9-CdS47\%$. $[MB] = 2.0 \times 10^{-5} M$.

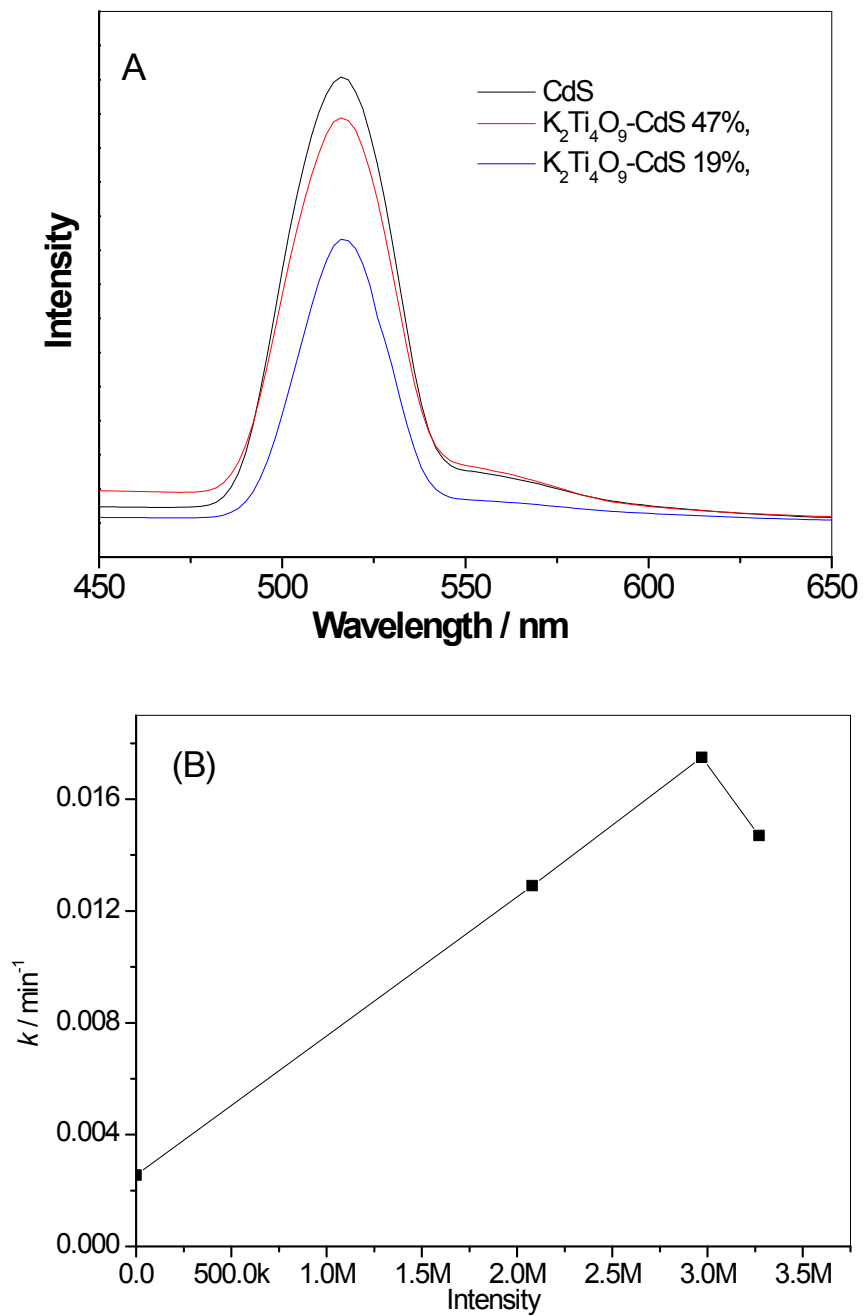


Fig. S9 (A) Photoluminescence spectra of CdS and composite $K_2Ti_4O_9$ -CdS with the excitation wavelength of 400 nm, (B) the correlation between rate constant and the photoluminescent intensity.

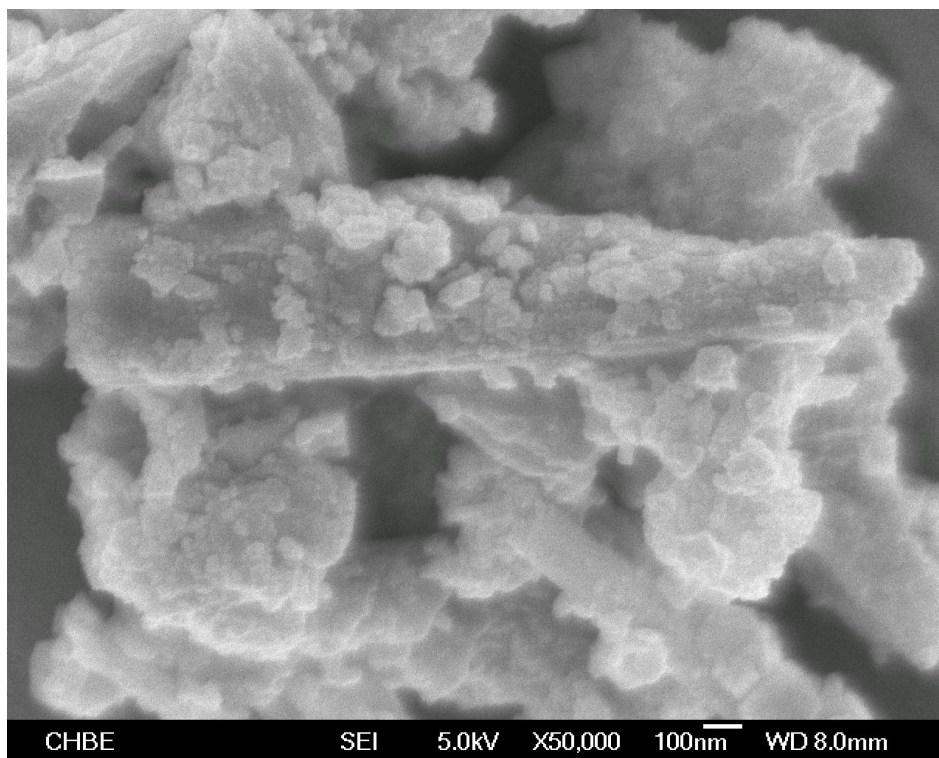


Fig. S10 FESEM image of sample K₂Ti₄O₉-CdS47%.